Chaotic dynamics in the rf superconducting quantum-interference-device magnetometer: A coupled quantum-classical system

J. Diggins, J. F. Ralph, T. P. Spiller, T. D. Clark, H. Prance, and R. J. Prance
Mathematical and Physical Sciences, University of Sussex, Falmer, East Sussex, BN1 9QH, United Kingdom
(Received 15 November 1993)

In this paper, we discuss the nonlinear behavior of a model rf superconducting quantum-interference-device magnetometer consisting of a macroscopic quantum object which is coupled reactively to a linear classical oscillator. We demonstrate that chaotic solutions can be found in the oscillator for the ground and first excited states of the quantum object over a wide range of parameters, including those relevant to experimental systems.

PACS number(s): 05.45.+b, 85.25.Dq

At its most basic level, the radio frequency superconducting quantum-interference-device (SQUID) magnetometer consists of a superconducting weak link ring and a simple LC oscillator circuit (the tank circuit) which is driven by an external current source, usually at radio frequencies (cf. Fig. 1) [1]. The current gives rise to a magnetic flux in the inductor, which couples via a mutual inductance M to the SQUID ring. This coupled magnetic flux induces a screening current in the ring which is, in turn, coupled back to the tank circuit.

The response of the weak link ring to an applied magnetic flux is periodic in integer units of the superconducting magnetic flux quantum $\Phi_0 = h/2e \simeq 2\times 10^{-15}$ Wb, and it is this periodicity which is used in the operation of the system as a magnetometer. The periodic nature of ring manifests itself by inducing the same periodicity in the oscillator through the mutual coupling. If a static (or quasistatic compared to radio frequencies) external magnetic flux is applied to the ring, the behavior of the oscillator will then depend on the value of the applied flux. The small value of Φ_0 then allows for very accurate determination of this external magnetic flux as the signal sweeps through many periods of Φ_0 [1].

However, this apparently simply system can give rise to complicated nonlinear behavior, including chaos. Using a classical model [2–4] for both the weak link ring and the oscillator, chaotic solutions to the resulting nonlinear differential equations have been found for the ring alone [5–7] and for the coupled system [8]. The appearance of chaotic behavior has also been reported in experimental rf-SQUID systems [9], and although such behavior is not particularly desirable in the operations of the system as a magnetometer, the existence of such experimental evidence means that it is an important tool in studying chaotic dynamics in real systems.

This purely classical model has been shown to be valid for weak link rings in the presence of inherent dissipation: due to the inclusion of a real resistor shunted across the weak link [1] or an effective resistance due to couplings to unprobed environmental degrees of freedom [10–12] such as those which introduce broadband noise [13]. However, when such inherent dissipation is not present, a quantum-mechanical model may be used for the ring, where the macroscopic coherence of the superconducting condensate allows the ring to be considered as a single macroscopic quantum degree of freedom [14,15] with the appropriate commutators [16]. This section approach to the problem of superconducting circuits has led to some remarkable experimental [17–25] and theoretical results [12,26–29] in the field of macroscopic quantum phenomena.

In particular, it has been shown that nonlinear [30] and chaotic behavior [31,32] can be obtained from a model rf-SQUID magnetometer consisting of a macroscopic quantum-mechanical weak link ring and a linear classical oscillator. In this paper we deal with the general behavior of such a system and consider the behavior of the classical oscillator in the presence of a ring in the ground state and the first excited state, and between the two extreme limits already discussed [30–32].

Our model rf-SQUID magnetometer therefore consists of a macroscopic quantum object (the weak link ring) and a linear classical oscillator (the tank circuit). The weak link ring is characterized by three parameters: the geometrical inductance of the ring (L_s), the capacitance of the weak link (C_s), and the (angular) frequency for Cooper pairs to tunnel across the weak link (ν). The weak link is then coupled inductively to the tank circuit

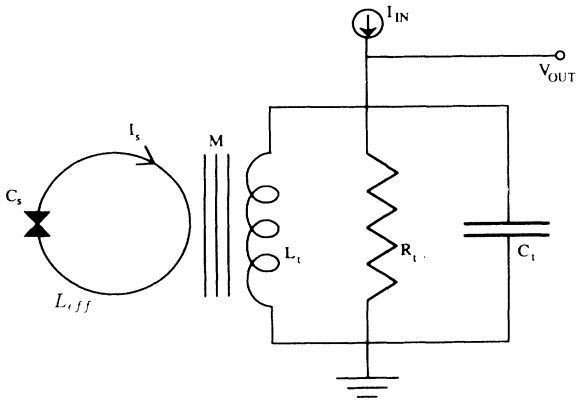

FIG. 1. Schematic diagram of the rf-SQUID magnetometer.

via a mutual inductance (M), where the tank circuit is taken to consist of a capacitor (C_t), and inductor (L_t), and a resistor (R_t) which are connected in parallel and driven by a current source $I_{IN}(t)$ (cf. Fig. 1).

In the absence of the ring, the behavior of the bare classical oscillator would be entirely linear. However, in the presence of the quantum object, a fraction of the magnetic flux threading the oscillator will be coupled into the ring, via M. This coupled magnetic flux will induce a screening current in the ring, which will in turn produce a magnetic flux which couples back to the oscillator, and so on. This type of reactive coupling is easily dealt with between two classical circuits [33], but here we have one quantum system and one classical system. The main obstacle to addressing this type of problem is that no generally excepted theory exists (as yet) to encompass both classical and quantum mechanics. However, approaching the problem from either side, by treating the classical oscillator as an infinite ensemble of quantum oscillators [34], or treating the ring as a classical circuit [2–4], it can be shown (Refs. [28] and [32], respectively) that the effect of this coupling is to renormalize the effective inductance of the ring by a factor $(1-K^2)$, where $K^2=M^2/L_tL_s$.

We can then use an analog of the Born-Oppenheimer approximation [35] from atomic physics to effectively integrate out the quantum degree of freedom. This approximation is frequently used in atomic physics to solve for the nucleic degrees of freedom by first solving for the electronic degrees of freedom, ignoring the dynamics of the nuclei, and then using the electronic energy states obtained to find the energy states of the nucleic motion [36]. If we assume that the fluctuations in the oscillator occur at a very much lower frequency than any fluctuations in the quantum object, we can solve for the quantum motion of the ring in an energy eigenstate and at a particular value of applied magnetic flux, and use the energy eigenvalue obtained to put back into the dynamics of the oscillator. This allows the dynamics of the ring to manifest themselves in the dynamics of the tank circuit while remaining adiabatically in an energy eigenstate.

The equation for the oscillator is then given by [29–32]

$$C_t\frac{d^2\Phi_t}{dt^2}+\frac{1}{R_t}\frac{d\Phi_t}{dt}+\frac{\Phi_t}{L_t} =I_{IN}(t)+\mu\langle\kappa|I_s(\Phi_{\rm dc}+\mu\Phi_t)|\kappa\rangle\ , \quad (1)$$

where Φ_t is the magnetic flux threading the oscillator, $\Phi_{\rm dc}$ is an applied static (or quasistatic) magnetic flux (external to the coupled system), $\mu=M/L_t$, and

$$\langle\kappa|I_s(\Phi_{\rm tot})|\kappa\rangle=-\frac{\partial E_\kappa(\Phi_{\rm tot})}{\partial\Phi_{\rm tot}} \quad (2)$$

is the expectation value of the screening current in the κth energy state, with energy eigenvalue $E_\kappa(\Phi_{\rm tot})$, and $\Phi_{\rm tot}=\Phi_{\rm dc}+\mu\Phi_t$ is the total applied flux (external to the ring).

To find the appropriate form for the screening current response it is then necessary to solve the time-independent Schrödinger equation for $E_\kappa(\Phi_{\rm tot})$ using the Hamiltonian for the SQUID ring [12,21,25,28–32]:

$$\mathcal{H}=\frac{Q_s^2}{2C_s}+\frac{(\Phi_s-\Phi_{\rm tot})^2}{2L_{\rm eff}}-\hbar\nu\cos\left[\frac{2\pi\Phi_s}{\Phi_0}\right], \quad (3)$$

where $L_{\rm eff}=L_s(1-K^2)$ is the effective (renormalized) inductance of the ring, and Q_s and Φ_s are the electric and magnetic flux operators which obey the commutator [16]

$$[Q_s,\Phi_s]=-i\hbar\ . \quad (4)$$

Using an appropriate representation for the Q_s operator, it is then possible to solve for the energy eigenvalue and for the screening current response at a general value of $\Phi_{\rm tot}$. In two extreme limits it is possible to solve the problem analytically, but in general numerical methods must be employed [12,37]. However, from the form of the Hamiltonian, it is possible to show that each energy eigenvalue $E_\kappa(\Phi_{\rm tot})$ (and hence the screening current response) will be periodic with period Φ_0 [28].

In the limit where $\hbar\nu\ll\hbar\omega_0$ [$\omega_0=(C_sL_s)^{-1/2}$], perturbation theory may be used to solve for the energy eigenvalue, using the simple harmonic-oscillator states as an unperturbed basis. This gives the screening current response a sinusoidal form [28,30], where the expectation values of the screening current are given by

$$\langle\kappa|I_s(\Phi_{\rm tot})|\kappa\rangle=-q\nu\sin\left[\frac{2\pi\Phi_{\rm tot}}{\Phi_0}\right]L_\kappa(2\pi^2\beta)e^{-\pi^2\beta}\ , \quad (5)$$

where $q=2e$, $\beta=\hbar\omega_0L_{\rm eff}/\Phi_0^2$, and $L_\kappa(x)$ is the Laguerre polynomial of order κ [38].

In the other extreme limit $\hbar\nu\gg\hbar\omega_0$, the screening

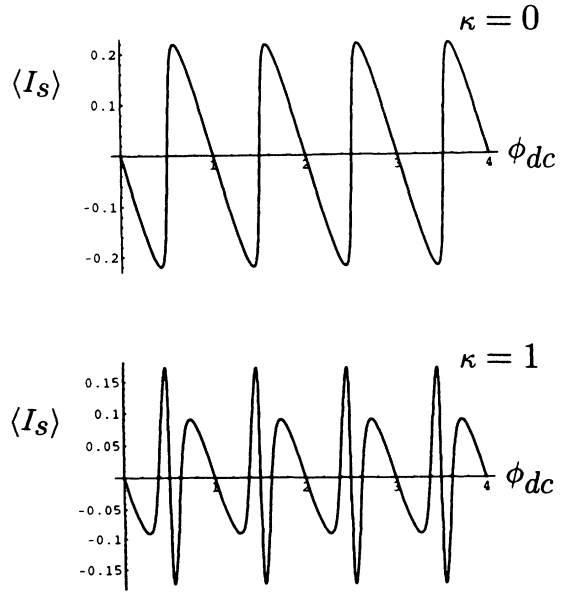

FIG. 2. Expectation value of screening current for the ground state and the first excited state, $(L_{\rm eff}/\Phi_0)\langle 0|I_s(\Phi_{\rm tot})|0\rangle$ and $(L_{\rm eff}/\Phi_0)\langle 1|I_s(\Phi_{\rm tot})|1\rangle$, respectively, for $\hbar\omega_0=0.043(\Phi_0^2/L_{\rm eff})$ and $\hbar\nu=0.055(\Phi_0^2/L_{\rm eff})$.

current response for the ground state approaches a perfect sawtooth, with negative linear branches [28,31,32] corresponding to the quantized flux states of the thick superconducting ring with no weak link [1];

$$\langle 0|I_s(\Phi_{\rm tot})|0\rangle=\frac{\Phi_0}{L_{\rm eff}\pi}\sum_{n=1}^{\infty}\frac{(-1)^n}{n}\sin\left[\frac{2\pi\Phi_{\rm tot}}{\Phi_0}\right]. \tag{6}$$

Unfortunately, between these two limits there is no analytic solution for the ground state or any of the excited states, and numerical methods must be used [28,37]. There numerical solutions give very distinctive features for the ground and first excited states (cf. Fig. 2). The ground-state screening current has the form of a clipped sawtooth, with the amount of clipping dependent on the relative values of ω_0 and ν, while the first excited state has a very distinctive wiggle for almost all values of the parameters, and all the values considered in this paper. Of course, the fact that the screening currents shown in Fig. 2 do not have a simple analytic expression does not mean that we cannot solve Eq. (1). In fact, we will use two different approximations which yield remarkably similar solutions.

If we represent the screening current functions by

$$\langle\kappa|I_s(\Phi_{\rm tot})|\kappa\rangle=-\frac{\Phi_0}{L_{\rm eff}}S_\kappa\left[\frac{\Phi_{\rm tot}}{\Phi_0}\right], \tag{7}$$

we can write (1) in terms of dimensionless quantities, where we define $\phi=\Phi_t/\Phi_0$, $\phi_{\rm dc}=\Phi_{\rm dc}/\Phi_0$, $Q=R_t(C_t/L_t)^{1/2}$, $i_{\rm in}(t)=[QM(1-K^2)^{1/2}(1+\alpha^2)^{-1/2}]I_{IN}(t)/\Phi_0$, $\alpha=K^2Q(1-K^2)^{-1/2}$, $\gamma=L_t/L_s$, and $2\pi\tau=\omega_r t$, and ω_r is the pseudoresonant frequency for the nonlinear oscillator for very small oscillations about $\phi_{\rm dc}=0$ [25]. This pseudoresonant frequency is found by linearizing around $\phi_{\rm dc}=0$, and is given by $\omega_r=g[C_tL_t(1-K^2)]^{-1/2}$, where

$$g=\left[1-K^2\left[1-\left.\frac{dS_\kappa(x)}{dx}\right|_{x=0}\right]\right]^{1/2}. \tag{8}$$

The system is then driven at this pseudoresonant frequency by a sinusoidal driving term, which is consistent with experiment [25,28].

The dimensionless equation for the oscillator then becomes

$$\frac{d^2\phi}{d\tau^2}+\left[\frac{2\pi(1-K^2)^{1/2}}{Qg}\right]\frac{d\phi}{d\tau}+\left[\frac{2\pi}{g}\right]^2[(1-K^2)\phi+\mu\gamma S_\kappa(\mu\phi+\phi_{\rm dc})]=(2\pi)^2\left[\frac{(1+\alpha^2)^{1/2}(1-K^2)^{1/2}}{Qg\mu}\right]i_{\rm in}\cos(2\pi\tau+\delta), \tag{9}$$

where δ is the initial phase for the driving term. This equation can then be solved numerically for any choice of screening current response, the five independent parameters (K, γ, Q, $i_{\rm in}$, and $\phi_{\rm dc}$), and the three initial conditions for ϕ, $d\phi/d\tau$, and δ.

Although it is possible to calculate $S_\kappa(x)$ very accurately by matrix diagonalization [37], the accurate numerical integration of (9) would require vast computing resources if the function were to be calculated for each step of the numerical solution. This is clearly impractical. We therefore resort to the use of two different approximations.

The first approximation is to generate a loop-up table for values of $S_\kappa(x)$ for different values of x. The periodicity of the screening current means that we need specify only the value of S_κ for arguments between zero and one. Points which fall between the values set in the look-up table can then be approximated by linear interpolation. Of course, the more points which are used to create this table, the more accurate the solution will be. In practice, very good results can be obtained by using several thousand points.

This method clearly introduces errors due to the interpolation, in addition to the ones inherent in the numerical solution. Periodic solutions tend to be less sensitive to such errors than are any chaotic solutions. The fractal nature of the basin of attraction of a chaotic solution means that such errors are often large enough to allow the system to escape the basin. Nevertheless, it is possible to follow chaotic trajectories for sufficiently long periods to estimate the Liapunov exponents, calculate the power spectra, and record their Poincaré sections.

The other approach used is to approximate the function $S_\kappa(x)$ by an analytic function which is constructed from a finite series of hyberbolic functions. The states of greatest interest are the ground and first excited states, which both have characteristic features for large ranges of parameters. Using this alternative approximation, the ground-state screening current S_0 is given by

$$S_0(x)=-s_{02}x+\frac{s_{02}}{2}\sum_{n=0}^{N}\{\tanh[s_{01}(n+\tfrac{1}{2}+x)]+\tanh[s_{01}(n-\tfrac{1}{2}-x)]\}-s_{03}\sin(2\pi x) \tag{10}$$

and the first excited state screening current by

$$S_1(x)=-s_{12}x+\frac{s_{12}}{2}\sum_{n=0}^{N}\{\tanh[s_{11}(n+\tfrac{1}{2}+x)]+\tanh[s_{11}(n-\tfrac{1}{2}-x)]\}+s_{13}\sum_{n=0}^{N}\{\tanh[s_{14}(n+\tfrac{1}{2}+x)]-\tanh[s_{15}(n+\tfrac{1}{2}+x)]+\tanh[s_{14}(n-\tfrac{1}{2}-x)]-\tanh[s_{15}(n-\tfrac{1}{2}-x)]\}-s_{16}\sin(2\pi x), \tag{11}$$

where the s parameters (s_{01}, s_{02}, s_{03}, s_{11}, etc.) can be least squares fitted to a corresponding screening current response which is calculated by matrix diagonalization, and N is a large integer (in practice, N need only be of the order of 10, provided the excursions in x are sufficiently small).

The usual way in which to represent the dynamics of this system is to plot the voltage response of the tank circuit against the amplitude of the forcing current, I_{IN} [1,28]. Here we give the component of the (dimensionless) voltage $v_{\rm in}$ which is in phase with the forcing current versus the dimensionless current amplitude $i_{\rm in}$, where,

$$v_{\rm in}=\frac{\mu}{\pi(1+\alpha^2)^{1/2}}\int_{-1/2}^{1/2}d\tau\frac{d\phi}{d\tau}\cos(2\pi\tau+\delta)\ . \qquad (12)$$

Figure 3 shows examples of these voltage characteristics for the ground and first excited states for two different values of the external dc magnetic flux $\phi_{\rm dc}=0$ and $\frac{1}{2}$, corresponding to the two extremes of the periodic response. The general features of these voltage characteristics are very similar for a wide range of ν and ω_0, including those which are appropriate for the physical systems. We consider typical experimental weak link niobium rings with capacitances and inductances of the order of 1×10^{-16} F and 0.3 nH, respectively, and tunnel currents of the order of $2e\nu=2$ μA [25]; giving $\hbar\omega_0\sim\hbar\nu\simeq0.05(\Phi_0^2/L_{\rm eff})$. We will also set $Q=50$ and $\gamma=400$ for simplicity, and to be in line with approximate experimental values [25].

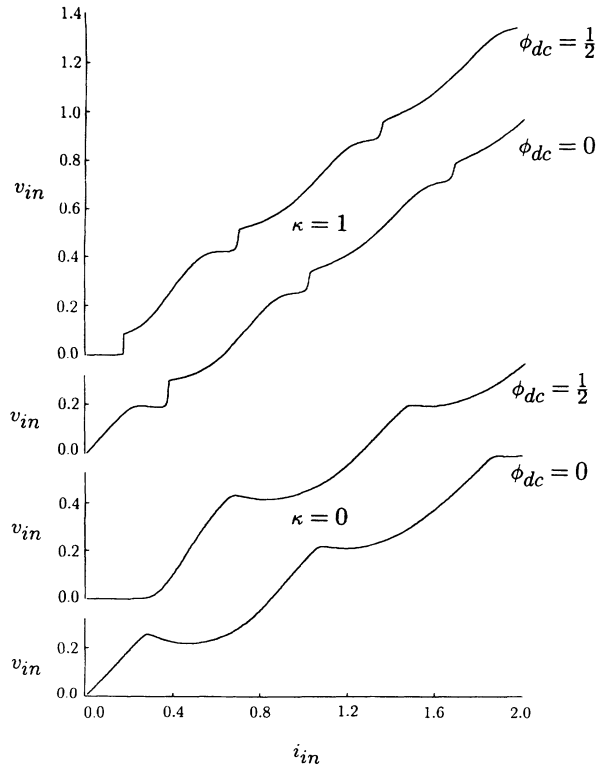

FIG 3. The in-phase voltage characteristics for the ground ($\kappa=0$) and first excited ($\kappa=1$) states for $\phi_{\rm dc}=0$ and $\phi_{\rm dc}=\frac{1}{2}$, with $K^2=0.03$ and the screening current responses shown in Fig. 2.

As the coupling between the two systems is increased, the effect of the nonlinearity becomes more pronounced. Chaotic and multiperiodic solutions have been found for the ground-state screening current response with a discontinuous sawtooth [31,32] for couplings $K^2>0.2$. Obviously, we would expect similar solutions to be present where the ground-state response was a very sharp continuous sawtooth; but where the sawtooth is somewhat rounded, as in Fig. 2, there need not be any chaotic or multiperiodic behavior for moderate values of the coupling, $K^2\simeq0.2$–0.3. Indeed, for the screening current responses shown in Fig. 2 there are no chaotic solutions for $K^2<0.3$ and $\phi_{\rm dc}=0$ for either the ground or first excited states. However, by changing the value of the external dc magnetic flux, it is possible to find chaotic solutions for couplings as low as $K^2\simeq0.04$ with $\phi_{\rm dc}=\frac{1}{2}$, which is well within the range of values accessible in experiments [25]. Figures 4(a) and 4(b) show Poincaré sections through two of these chaotic solutions for different values of the forcing current. We have chosen a coupling of $K^2=0.15$ where there is no competition from other attractors allowing an accurate determination of the Liapunov exponents $\lambda=(+,0,-)$ [also shown in Figs. 4(a) and 4(b)] and their power spectra [shown in Figs. 4(c) and 4(d)]. It is worth noting that while the solutions shown in Fig. 4 were generated using the hyperbolic approximation (9), a look-up table with 1000 points will give results which are indistinguishable to the naked eye. These chaotic solutions appear for a wide range of couplings $K^2>0.04$ and are not too sensitive to the precise value of the dc flux, they appear stable for $0.41\le\phi_{\rm dc}\le0.59$. The two power spectra, shown in Figs. 4(c) and 4(d), give the dimensionless quantities $\ln[\bar{v}^2(\hat{\omega})]$ versus $\hat{\omega}$ and are related to the actual mean-squared voltage $\bar{V}^2(\omega)$ (in real voltage units) and angular frequency ω by

$$\hat{\omega}=2\pi\sqrt{1-K^2}(\omega/\omega_R),$$

$$\bar{v}^2(\hat{\omega})=4\pi^2(1-K^2)[\bar{V}^2(\omega)/\Phi_0\omega_R]\ ,$$

where $\omega_R=\sqrt{C_tL_t}$ is the resonant frequency of the bare tank circuit. These spectra have two main features. Each spectrum has a single-frequency component corresponding to the frequency of the forcing term (along with some minor contribution from higher harmonics) and a continuous background spectrum which is associated with chaotic behavior. The continuous background spectrum has a rough peak to the low-frequency side of the main resonance. This peak is characteristic of all the chaotic solutions found for the ground state, and is very much broader than the width of the resonant peak, which is given by the Q value for linear oscillators. These spectra are shown since they are possible candidates for experimental investigation [39].

Figure 5 shows the Poincaré section of another chaotic attractor, this time for a slightly sharper sawtooth response with $\hbar\nu=0.075(\Phi_0^2/L_{\rm eff})$ and $\hbar\omega_0=0.043(\Phi_0^2/L_{\rm eff})$. By blowing up a small window (shown in the inset), we can see some of its fractal structure, and this fine detail also allows the calculation of the fractal, information, and correlation dimensions of the attractor.

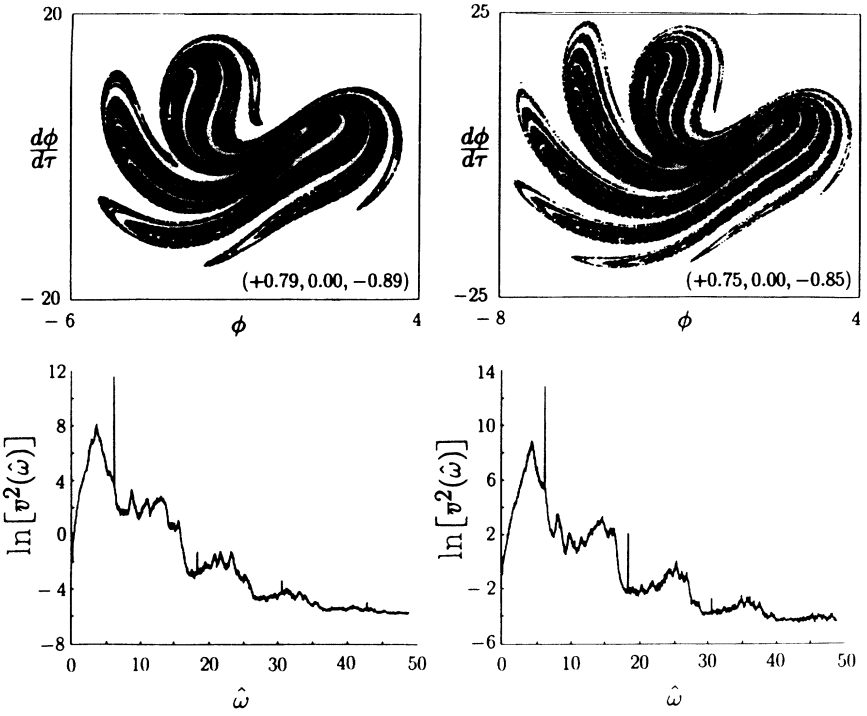

FIG. 4. Poincaré sections and frequency spectra of chaotic solutions found for the ground-state screening current response shown in Fig. 2, $K^2=0.15$, $\phi_{dc}=0.5$, and for $i_{in}=0.1$ [Figs. 4(a) and 4(c)] or $i_{in}=0.15$ [Figs. 4(b) and 4(d)].

For the solution shown in Fig. 5 these are $D_f=0.180\pm0.01$, $D_i=0.182\pm0.01$, and $D_c=0.181\pm0.01$, respectively.

In the first excited state chaotic and multiperiodic solutions still occur, but they are not as common at low couplings as those found for the ground state. Such solutions also require a screening current response which is much sharper than that shown in Fig. 2. An example of one of these chaotic solutions (or at least its Poincaré section) is shown in Fig. 6. This particular solution was generated using a screening current corresponding to $\hbar\nu=0.085(\Phi_0^2/L_{\text{eff}})$. This is higher than that used to generate the chaotic solutions found for the ground state, but it is still comparable with the typical experimental value which we quoted above [25]. Whereas the chaotic solutions for the ground state response are found when the dc flux is biased at around $\phi_{dc}=0.5$, the first excited state tends to give chaotic solutions when $\phi_{dc}\simeq0.4$ corresponding to oscillations around the wiggle in the screening current response (cf. Fig. 2).

In this paper, we have shown that it is possible to obtain chaotic behavior in our model rf-SQUID magnetometer, consisting of a linear classical oscillator coupled to a macrosopic quantum object. Chaotic solutions have been shown to exist for both the ground and first excited states and for a wide range of parameter values.

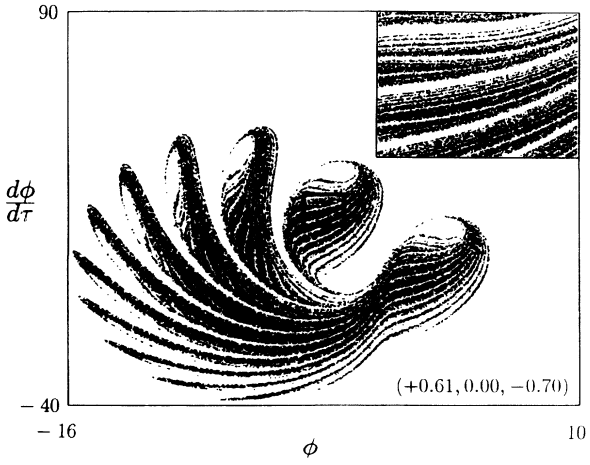

FIG. 5. Poincaré section of a chaotic solution found for the ground state with $\hbar\nu=0.075(\Phi_0^2/L_{\text{eff}})$, $\hbar\omega_0=0.043(\Phi_0^2/L_{\text{eff}})$, $\phi_{dc}=0.5$, $K^2=0.15$, and $i_{in}=0.25$. The inset shows some of the fractal structure of the Poincaré section in more detail.

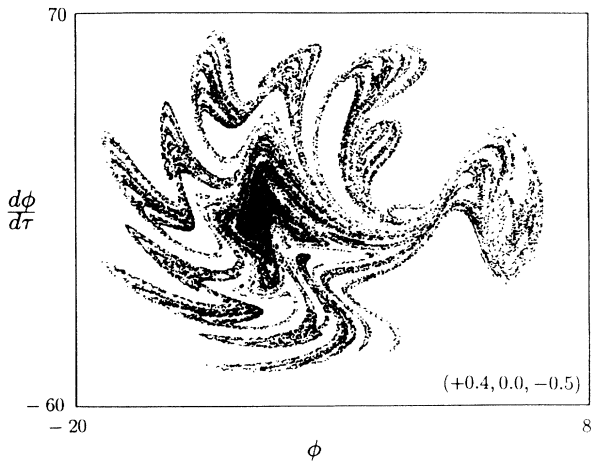

FIG. 6. Poincaré section of a chaotic solution found for the first excited state with $\hbar\nu=0.085(\Phi_0^2/L_{\text{eff}})$, $\hbar\omega_0=0.043(\Phi_0^2/L_{\text{eff}})$, $\phi_{dc}=0.4$, $K^2=0.3$, and $i_{in}=0.18$.

Of course, it is not entirely surprising that a nonlinear oscillator equation such as (9) will give rise to chaotic solutions for some range of parameter values. What is important is that the range of parameters for which such solutions exist is in a physically accessible region of the whole parameter space. Indeed, we have found that there are many chaotic solutions within the range of typical experimental systems.

Also, the nature of the nonlinearity in this case is quite unique. Our system is part classical and part quantum mechanical, and it is the effect of the macroscopic quantum object on the classical oscillator which leads to the appearance of nonlinear behavior in the otherwise linear oscillator. The quantum-mechanical origin of the nonlinearity can then lead to other interesting possibilities. It has been suggested that the dependence of the nonlinearity, and hence the nonlinear dynamics of the oscillator, on the energy state of the quantum object could be used to identify transitions between otherwise indistinguishable energy states by varying one of the control parameters quasistatically and looking at the change in the dynamical response [30]. Here, where the voltage characteristics of the ground and first excited states are distinguishable (cf. Fig. 3), it might be possible to identify transitions between states without the need to generate the entire voltage characteristic, possibly by looking at changes in the power spectrum.

The authors would like to thank the Science and Engineering Research Council, the National Physical Laboratory, and the Royal Society for their generous funding of this work. We would also like to thank Professor F. Brouers for useful and informative discussions in the preparation of this paper.

[1] A. Barone and G. Paterno, *Physics and Applications of the Josephson Effect* (Wiley, New York, 1982).
[2] D. E. McCumber, J. Appl. Phys. **39**, 3113 (1968).
[3] W. C. Stewart, Appl. Phys. **12**, 277 (1968).
[4] W. J. Johnson, Ph.D. thesis, University of Wisconsin, 1968.
[5] M. P. Soerensen, M. Bartucelli, P. L. Christiansen, and A. R. Bishop, Phys. Lett. **109A**, 347 (1985).
[6] W. C. Schieve, A. R. Bulsara, and E. W. Jacobs, Phys. Rev. A **37**, 3541 (1988).
[7] E. W. Jacobs, A. R. Bulsara, and W. C. Schieve, Physica D **34**, 439 (1989).
[8] S. A. Bulgakov, V. B. Ryabov, V. I. Shnyrkov, and D. M. Vavriv, J. Low. Temp. Phys. **83**, 241 (1991).
[9] I. Dmitrenko, D. A. Konotop, G. M. Tsoi, and V. I. Shnyrkov, Fiz. Nizk. Temp. **9**, 666 (1983) [Sov. J. Low Temp. **9**, 340 (1983)].
[10] A. O. Caldeira and A. J. Leggett, Phys. Lett. **46**, 211 (1981).
[11] A. O. Caldeira and A. J. Leggett, Ann. Phys. **149**, 375 (1983).
[12] T. P. Spiller, T. D. Clark, R. J. Prance, H. Prance, D. A. Poulton, Nuovo Cimento **105B**, 749 (1990).
[13] R. J. Prance, J. E. Mutton, E. P. Shepard, T. D. Clark, H. Prance, and T. P. Spiller, in *SQUID '85: Proceedings of the 3rd International Conference on Superconducting Devices, 1985,* edited by H. D. Hahlbohm and M. Lübbig (Walter de Gruyter, Berlin, 1985), p. 151.
[14] R. P. Feynman, *The Feynman Lectures on Physics* (Addison-Wesley, Reading, MA, 1966), Vol. III, Chap. 21.
[15] A. Widom, T. D. Clark, G. Megaloudis, and G. Sacco, Nuovo Cimento **61B**, 112 (1981).
[16] A. Widom, J. Low Temp. Phys. **37**, 449 (1979).
[17] R. J. Prance, J. E. Mutton, H. Prance, T. D. Clark, A. Widom, and G. Megaloudis, Helv. Phys. Acta **56**, 789 (1983).
[18] J. E. Mutton, R. J. Prance, and T. D. Clark, Phys. Lett. **104A**, 375 (1984).
[19] M. H. Devoret, D. Esteve, J. M. Martinis, and J. Clarke, Phys. Rev. Lett. **53**, 1260 (1984).
[20] H. Prance, T. P. Spiller, J. E. Mutton, R. J. Prance, T. D. Clark, and R. Nest, Phys. Lett. **115A**, 125 (1986).
[21] T. D. Clark, in *Solid State Science: Past, Present and Predicted,* edited by D. L. Wearie and C. G. Windsor (Hilger, London, 1987), Chap. 8.
[22] J. M. Martinis, M. H. Devoret, and J. Clarke, Phys. Rev. B **35**, 4682 (1987).
[23] M. H. Devoret, D. Esteve, J. M. Martinis, A. N. Cleland, and J. Clarke, Phys. Rev. B **36**, 58 (1987).
[24] J. Clarke, A. N. Cleland, M. H. Devoret, D. Esteve, and J. M. Martinis, Science **239**, 992 (1988).
[25] R. J. Prance, T. P. Spiller, H. Prance, T. D. Clark, J. F. Ralph, A. J. Clippingdale, Y. Srivastava, and A. Widom, Nuovo Cimento B **106**, 431 (1991).
[26] A. J. Leggett, in *Proceedings of the International Symposium on the Foundations of Quantum Mechanics,* edited by S. Kamefuchi (Physical Society of Japan, Tokyo, 1983), p. 74.
[27] A. J. Leggett, *Proceedings of the 1983 Advanced Study Institute on Percolation, Localization and Superconductivity* (Pergamon, New York, 1984).
[28] T. P. Spiller, D. A. Poulton, T. D. Clark, R. J. Prance, and H. Prance, Int. J. Mod. Phys. B **5**, 749 (1990).
[29] T. P. Spiller, T. D. Clark, R. J. Prance, and A. Widom, Prog. Low Temp. Phys. **8**, 219 (1992).
[30] J. F. Ralph, T. P. Spiller, T. D. Clark, H. Prance, and R. J. Prance, Physica D **63**, 1991 (1993).
[31] J. F. Ralph, T. P. Spiller, T. D. Clark, R. J. Prance, and H. Prance, Phys. Lett. **180A**, 56 (1993).
[32] J. F. Ralph, T. P. Spiller, T. D. Clark, R. J. Prance, and H. Prance (unpublished).
[33] B. I. Bleaney and B. Bleaney, *Electricity and Magnetism,* 3rd ed. (Oxford University Press, Oxford, 1976).
[34] R. P. Feynman and F. L Vernon, Jr., Ann. Phys. **24**, 188 (1963).
[35] M. Born, Z. Phys. **38**, 803 (1926).
[36] L. I. Schiff, *Quantum Mechanics,* 3rd ed. (McGraw-Hill, New York, 1975).
[37] J. Diggins, T. P. Spiller, T. D. Clark, H. Prance, R. J. Prance, J. F. Ralph, B. Van den Bossche, and F. Brouers (unpublished).
[38] *Handbook of Mathematical Functions,* edited by M. Abramowitz and I. Stegun (Dover, New York, 1965).
[39] R. Whiteman, M. Brooks, R. J. Prance, T. D. Clark, H. Prance, T. P. Spiller, J. Diggins, A. J. Clippingdale, J. F. Ralph, Y. Srivastava, A. Widom, and F. Brouers (unpublished).

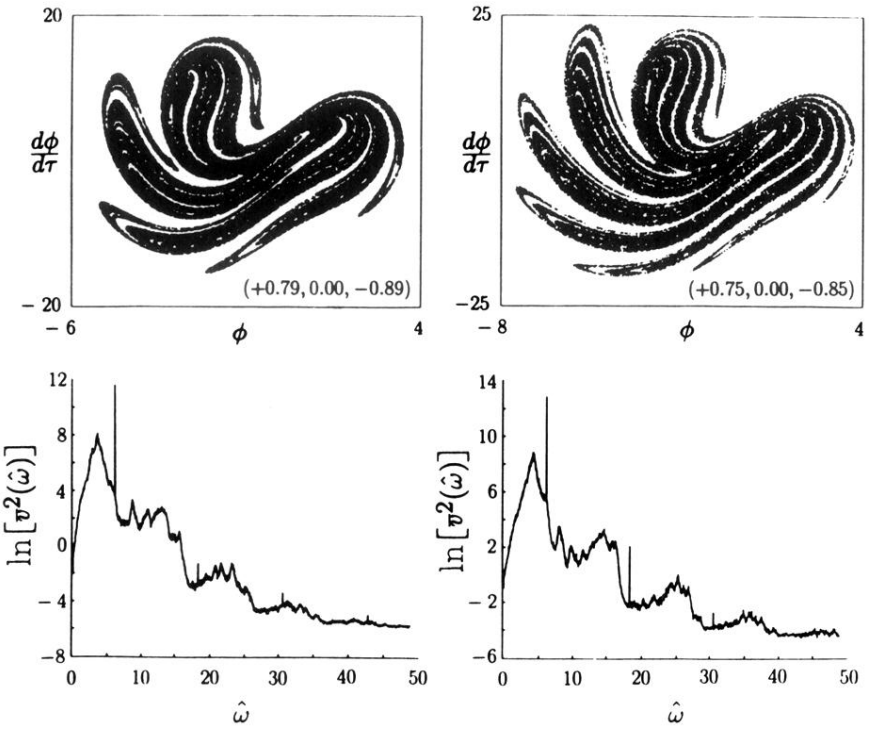

FIG. 4. Poincaré sections and frequency spectra of chaotic solutions found for the ground-state screening current response shown in Fig. 2, $K^2=0.15$, $\phi_{dc}=0.5$, and for $i_{in}=0.1$ [Figs. 4(a) and 4(c)] or $i_{in}=0.15$ [Figs. 4(b) and 4(d)].

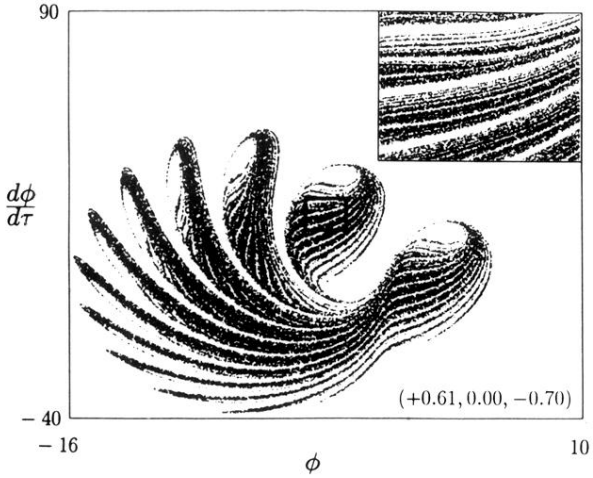

FIG. 5. Poincaré section of a chaotic solution found for the ground state with $\hbar\nu=0.075(\Phi_0^2/L_{\text{eff}})$, $\hbar\omega_0=0.043(\Phi_0^2/L_{\text{eff}})$, $\phi_{\text{dc}}=0.5$, $K^2=0.15$, and $i_{\text{in}}=0.25$. The inset shows some of the fractal structure of the Poincaré section in more detail.

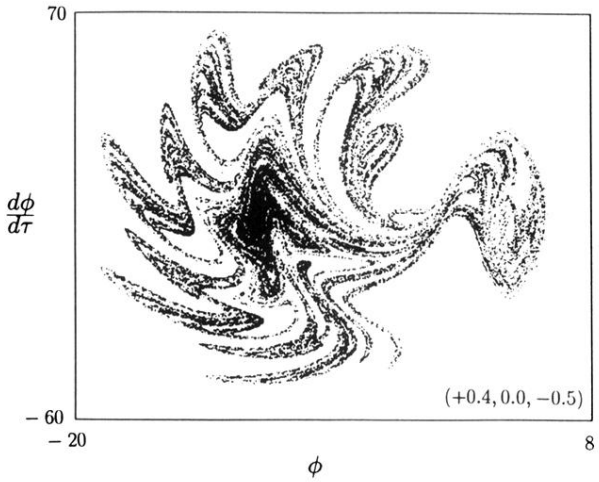

FIG. 6. Poincaré section of a chaotic solution found for the first excited state with $\hbar\nu = 0.085(\Phi_0^2/L_{\text{eff}})$, $\hbar\omega_0 = 0.043(\Phi_0^2/L_{\text{eff}})$, $\phi_{\text{dc}} = 0.4$, $K^2 = 0.3$, and $i_{\text{in}} = 0.18$.